ELSEVIER

Current Applied Physics 2 (2002) 465–471

Current Applied Physics
Physics, Chemistry and Materials Science

www.elsevier.com/locate/cap

Transport at surface nanostructures measured by four-tip STM ☆

Shuji Hasegawa *, Ichiro Shiraki, Fuhito Tanabe, Rei Hobara

Department of Physics, School of Science, University of Tokyo, 7-3-1 Hongo, Bunkyo-ku, Tokyo 113-0033, Japan

Received 8 May 2002; accepted 17 September 2002

Abstract

For in situ measurements of local electrical conductivity of well-defined crystal surfaces in ultrahigh vacuum, we have developed two kinds of microscopic four-point probe methods. One is a 'four-tip STM prober', in which independently driven four tips of scanning tunneling microscope (STM) are used for four-point probe conductivity measurements. The probe spacing can be changed from 500 nm to 1 mm. The other one is monolithic micro-four-point probes, fabricated on silicon chips, whose probe spacing is fixed around several μm. These probes were installed in scanning-electron-microscopy/electron-diffraction chambers, in which the structures of sample surfaces and probe positions were in situ observed. The probes can be positioned precisely on aimed areas on the sample with aid of piezo-actuators. With these machines, the surface sensitivity in conductivity measurements has been greatly enhanced compared with macroscopic four-point probe method. Then the conduction through the topmost atomic layers (surface-state conductivity) and influence of atomic steps upon conductivity could be directly measured. The STM prober is mainly described here.

PACS: 73.25.+I; 68.35.Bs; 68.37.Ef; 68.37.Hk
Keywords: Surface conductivity; Surface reconstruction; Scanning tunneling microscopy; Scanning electron microscopy

1. Introduction

The topmost layers of crystal surfaces are known to have characteristic electronic band structures that are sometimes quite different from in the inner bulk. While such *surface states* are well studied so far by e.g. photoemission spectroscopy and scanning tunneling spectroscopy, the electrical conduction through them, *surface-state conductance*, is little studied because of its difficulty [1]. Due to its thinness of the surface atomic layers, the surface-state conductance is usually much lower than the conductance through the underlying bulk crystal. Furthermore, surface defects like steps and domain boundaries greatly perturb the electron conduction through the surface states. These facts have prohibited the direct detection and quantitative measurement of the surface-state conductivity. Since, however, the surface-state conductance, electron conduction through only one or two atomic layers, is a key and essential issue in the study of electronic transport in nanometer-scale regions or objects, it has recently attracted much interest, and large amounts of efforts are now putting in for detecting and measuring it. Here we introduce a novel tool, *microscopic four-point probes*, and also demonstrate their effectiveness for such purposes [2–5].

First, we briefly introduce the principle of four-point probe method and electrical conduction near a semiconductor surface. As shown in Fig. 1(a), the outer pair of probes touches a sample surface and a voltage is applied between them, resulting in a current I flowing through the sample. The inner pair of probes picks up a voltage drop V along the surface due to the resistance of the sample. Thus one can obtain a four-point-probe resistance $R = V/I$ (strictly speaking, it is multiplied by a correction factor depending on the specimen shape and probe arrangement). Owing to this configuration, one can correctly measure the resistance of a sample without any influence of contact resistance at the probe contacts, irrespective of whether the probe contacts are ohmic or Schottky-type. This is because no current flows through the inner pair of contacts, so that no voltage

☆ Original version presented at QTSM & QFS '02 (Multilateral Symposium between the Korean Academy of Science and Technology and the Foreign Academies), Yonsei University, Seoul, Korea, 8–10 May 2002.

* Corresponding author. Tel./fax: +81-3-5841-4167.
E-mail address: shuji@surface.phys.s.u-tokyo.ac.jp (S. Hasegawa).

1567-1739/02/$ - see front matter © 2002 Published by Elsevier Science B.V.
PII: S1567-1739(02)00160-8

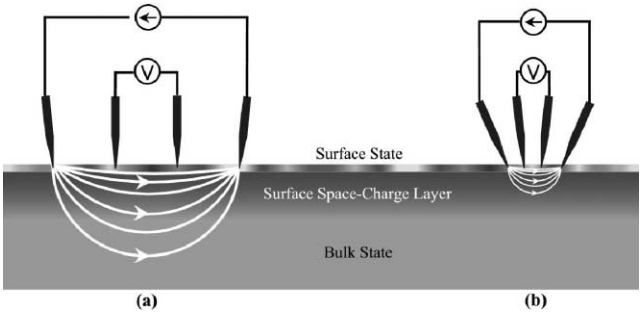

Fig. 1. (a) Macro- and (b) micro-four-point probe methods to measure electrical conductance. The distribution of current flowing through a semiconductor specimen is also schematically drawn.

drops at the probe contacts occur. This is a great advantage in the four-point probe method.

When the specimen is a semiconductor crystal, the measurement current will in principle flow through three channels in the sample [6]; (1) *surface states* on the topmost atomic layers (when a well-ordered surface structure is developed), (2) bulk states in the *surface space-charge layer* beneath the surface (when the bulk bands bend beneath the surface, the carrier concentration can be different from in the inner bulk), and (3) bulk states in the interior of crystal (which do not depend on the surface structures and states).

In general, the resistance measured by the four-point probe method contains the contributions from all of the three channels, and it is difficult to separate them. In the case of measurements in air, however, the sample surface is usually dirty and does not have a well-ordered surface structure, so that the measured resistance is interpreted to be only the bulk value. But under special conditions where the bands bend sharply under the surface to produce a carrier accumulation layer, or in ultrahigh vacuum (UHV) where the sample crystal has a well-defined surface superstructure to produce a conductive surface-state band, the contributions from the surface layers cannot be ignored. Even under such situations, however, the surface contributions have been considered to be very small, because, as shown in Fig. 1(a), the measurement current flows mainly through the underlying bulk in the case of *macroscopic* probe spacing.

Then, if one makes the probe spacing as small as the thickness of the space-charge layer or less, as shown in Fig. 1(b), the measurement current will mainly pass through the surface region only, to eliminate the bulk contribution in resistance measurement. This *microscopic four-point probe* method thus has a higher surface sensitivity. But, this picture looks too naïve, because the real current distribution may be complicated due to a possible barrier between the surface state and bulk state and/or a possible pn junction between the surface space-charge layer and underlying bulk state. But the experimental results described below will qualitatively show the validity of this intuitive picture in Fig. 1.

Microscopic four-point probes have another advantage; it enables local measurements by selecting the area under concern with aid of microscopes, so that the influence of defects can be avoided or intentionally included. Furthermore, by scanning the probes laterally on the sample surface, one can obtain a map of conductivity with a high spatial resolution [7]. Here a four-tip STM (scanning tunneling microscope) prober is introduced with some preliminary data.

2. Apparatus

Fig. 2 shows a series of scanning electron micrographs (SEM) of the four tips during the operation of the four-tip STM prober [4]. The tips are chemically etched W wires. While the probe spacing is as large as 1 mm in Fig. 2(a), the probes are brought together into about 1 μm spacing in Fig. 2(b)–(d). This apparatus enables STM operation by each tip independently, and

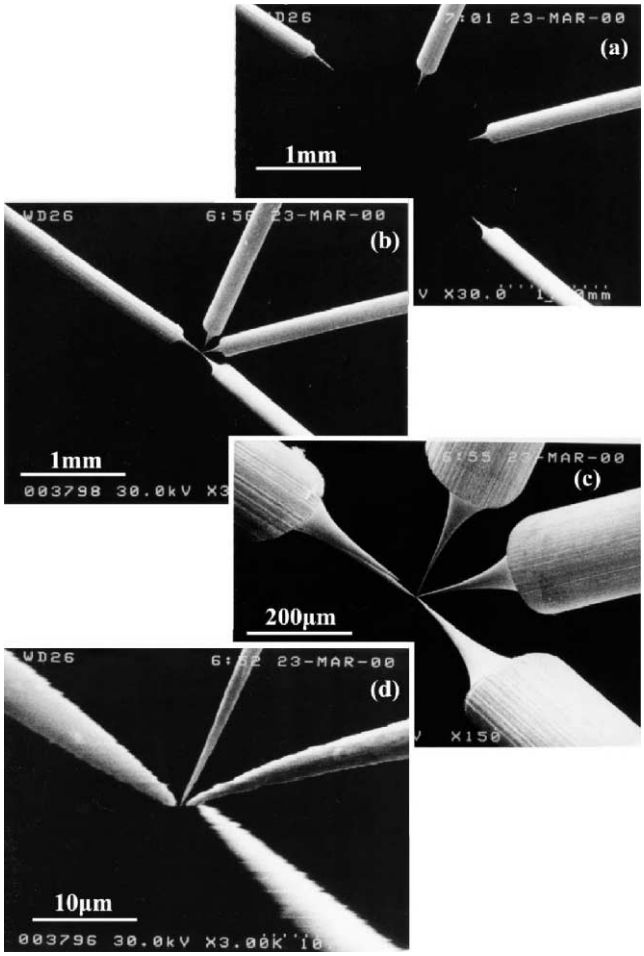

Fig. 2. SEM images of four tips of the independently driven four-tip STM prober.

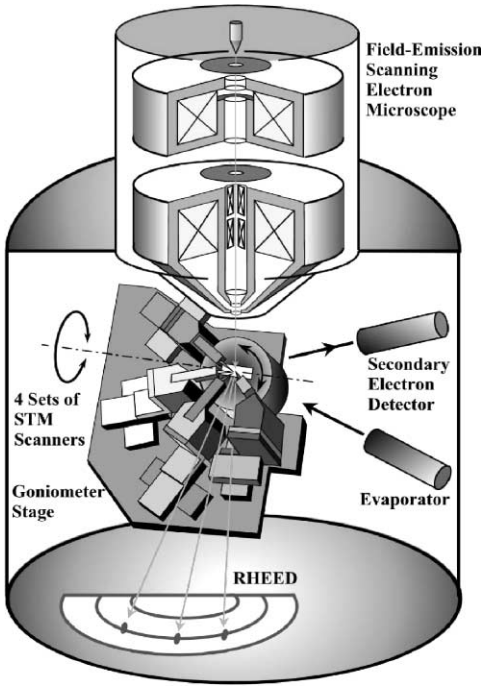

Fig. 3. A schematics of the independently driven four-tip STM prober, installed in an UHV–SEM–RHEED system.

also four-point probe conductivity measurements with various probe arrangements and spacing. The four tips are made approach to the sample surface simultaneously with feedback control by tunnel current detection. After that, the tips are made forward by a definite distance by piezo-actuators to make direct contacts to the sample surface, and then the four-point-probe conductivity measurement is done. The pre-amplifier is swiftly switched from the tunnel current mode to the four-point probe conductivity measurement mode.

Fig. 3 is a schematic of the apparatus in an ultrahigh vacuum (UHV) chamber. Each tip points to the sample with 45° from the sample surface, and is driven by a special type of piezo-scanner for fine positioning and by three sets of piezo-actuators (Microslide, Omicron) for coarse motion. The goniometer stage enables parallel shifts in three directions and tilt rotation around an axis. The sample can be rotated azimuthally by 360° with respect to the stage.

These positioning mechanisms enable fine adjustments with respect to the SEM electron beam, to do reflection-high-energy electron diffraction (RHEED) and scanning reflection electron microscopy (SREM) observations of the sample surface simultaneously. These supplementary electron microscopy/diffraction techniques are indispensable not only for positioning the four tips properly, but also for confirming the surface structures of sample. The tips and sample can be exchanged and installed by transfer rods without breaking vacuum.

The STM images by each tip do not yet have atomic resolutions, but monatomic steps are resolved. The details of this apparatus are described in Ref. [4].

3. Probe-spacing dependence

We shall introduce some results for two typical surface structures on a Si(1 1 1) crystal. One is Si(1 1 1)-7×7 clean surface, obtained by flash heating up to 1250 °C in UHV, and another is Si(1 1 1)-$\sqrt{3} \times \sqrt{3}$-Ag superstructure, obtained by depositing one atomic layer of Ag on the 7×7 surface kept at 450 °C. Their atomic arrangements and surface electronic states are already well understood; the details are in e.g., Refs. [1,8]. The latter surface has a two-dimensional free-electron-like metallic surface-state band, while the former surface has a localized metallic surface state (dangling-bond state). Since the characters of their electronic structures are so different, they thus provide comparative testing grounds for the surface conductance measurement.

Fig. 4(a) and (b) show the results for the respective surfaces at room temperature (RT) in UHV obtained at a four-tip arrangement of 5 μm spacing. The sample Si crystal was $3 \times 15 \times 0.4$ mm^3 in size, n-type, 5–15 Ω cm

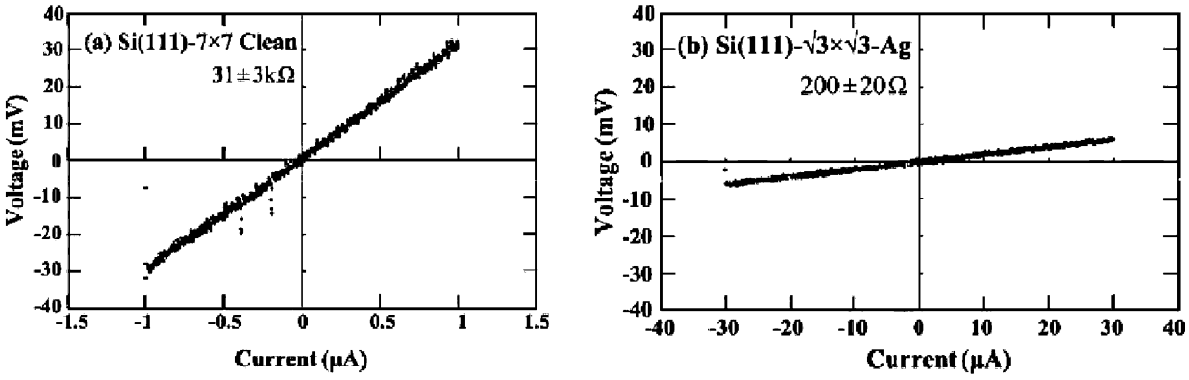

Fig. 4. *I–V* curves measured at room temperature with the four-tip STM prober at probe spacing of 5 μm for (a) Si(1 1 1)-7×7 clean and (b) Si(1 1 1)-$\sqrt{3} \times \sqrt{3}$-Ag surfaces, respectively. By fitting the curve by a straight line, the differential resistance is obtained from its gradient.

in bulk resistivity. The voltage drop measured by the inner pair of probes (in vertical axis) is linearly proportional to the current fed through the outer pair of probes (in horizontal axis). From the gradients of the curves, the differential resistance is obtained to be 31 ± 3 kΩ for the 7×7 surface and 200 ± 20 Ω for the $\sqrt{3} \times \sqrt{3}$-Ag surface. The error bars mean data scattering depending on the measured areas on the respective surfaces.

Only one atomic-layer of Ag deposited on a Si crystal of 0.4 mm thick makes the electrical resistance decrease by more than two orders of magnitudes! Many of the readers cannot believe this result at once. But we confirmed the reproducibility with several samples, and had confirmed its validity from the additional data described below. By comparing this result with the previous ones by macroscopic four-point probes of about 10 mm probe spacing in which the difference in resistance between the two surfaces was only around 10% [9], it is evident that *the miniaturization of four-point probes makes the resistance measurements very sensitive to the surface structures*. This is the expectation in Fig. 1.

In order to confirm this result further, we did the systematic four-point probe measurements by changing the probe spacing from 1 mm to 1 μm; the four tips can be independently driven in this machine, so that we can arrange the probes arbitrarily on the sample surface to make the probe spacing change continuously. The result is shown in Fig. 5 [4]. The horizontal axis is the probe spacing d, and the vertical axis is the differential resistance derived from the IV curves similar to those in Fig. 4 (the values are without corrections by multiplying the geometrical factor). Data points of filled circles are for the 7×7 clean surface, and filled squares are for the $\sqrt{3} \times \sqrt{3}$-Ag surface. This clearly shows that the probe-spacing dependence of resistance is quite different between the two surfaces. For the 7×7 surface, the resistance changes significantly in a characteristic way depending on the probe spacing; especially it drastically increases at $d < 10$ μm. For the $\sqrt{3} \times \sqrt{3}$-Ag surface, on the other hand, the change in resistance is much more moderate; the resistance gradually decreases with decreasing d, which is opposite to the tendency for the 7×7 surface. *These differences mean that the nature of electron conduction is quite different between the two surfaces*. While the difference in resistance between the two surfaces is negligibly small at $d \sim 1$ mm, the difference becomes as large as two or three orders of magnitudes at $d < 10$ μm. This evidently shows the expectation in Fig. 1; as the probe spacing is reduced, the measurement has a higher surface sensitivity. The results with smaller probe spacings should be more intrinsic to the surface structures because of negligible contribution from the bulk region.

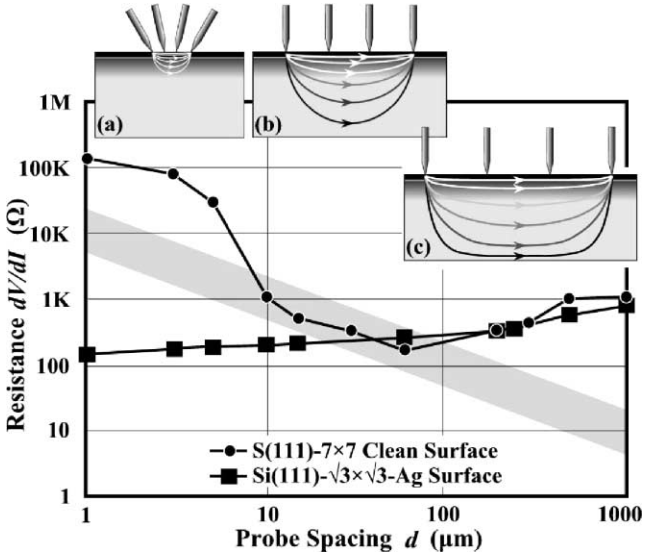

Fig. 5. Probe-spacing dependence of the resistance of a Si crystal, measured at room temperature by the independently driven four-tip STM prober, for Si(1 1 1)-7×7 clean surface (●) and Si(1 1 1)-$\sqrt{3} \times \sqrt{3}$-Ag surface (■). The insets are schematic illustrations of the current distribution in the sample for the case of the 7×7 surface.

The results are qualitatively described by Ohm's law in classical electromagnetism. If we assume the sample as a homogeneous semi-infinite three-dimensional resistive material, the measured resistance R should be written by

$$R = \rho/2\pi d, \tag{1}$$

where ρ is its bulk resistivity (Ω cm). The resistance should be inversely proportional to the probe spacing d. This relation is shown in Fig. 5 by a shaded band, because our Si sample has the resistivity of $\rho = 5$–15 Ω cm. The experimental data for the 7×7 surface are consistent with this theoretical prediction only at 10 μm $< d <$ 100 μm, while the data points deviate upward from the theory at larger d and smaller d. This feature with comparison to Eq. (1) was confirmed also for silicon crystals of different bulk resistivities. Therefore, we can say that the sample crystal (0.4 mm thick) is regarded as a homogeneous semi-infinite bulk when the probe spacing d is between 10 and 100 μm, because the current distribution does not practically reach to the bottom of the crystal as schematically shown by the inset (b) in Fig. 5. The influence of surface is negligible, because the majority of the measuring current passes through the bulk region.

When d is larger ($d > 100$ μm), on the other hand, the current penetrates deeper in the crystal and reaches to its bottom as show in the inset (c) of Fig. 5; the current distribution may be compressed due to the finite thickness of the sample. This effectively raises the measured resistance. This corresponds to the data points at $d > 100$ μm, deviating upward from the prediction of Eq. (1).

At smaller d regime ($d < 10$ μm), which is comparable to the thickness of the surface space-charge layer

(~1 μm), on the contrary, the current flows only near the surface as shown in the inset (a); the penetration depth of the current distribution in the sample is similar to the probe spacing in usual cases. Therefore, the data points in Fig. 5 indicate that the resistance at the surface region of the sample is larger than that of the inner bulk, because the data at $d < 10$ μm deviate upward form the shaded band. This conclusion is reasonable when one recalls a fact that the surface space-charge layer beneath the clean 7×7 surface is always a depletion layer, irrespective of the bulk doping concentration and type, because the Fermi level is pinned by the dangling-bond state located at the middle of the band gap [10,11]. Thus the surface region has a higher resistance for the 7×7 surface.

On the other hand, the d dependence of resistance for the $\sqrt{3} \times \sqrt{3}$-Ag surface does not fit Eq. (1) at all. According to Ohm's law in classical electromagnetism, when the resistance of an infinite two-dimensional sheet is measured by a four-point probe of probe spacing d, the measured resistance R is written as

$$R = (\ln 2/2\pi) \cdot R_S, \tag{2}$$

where R_S is the sheet resistance (Ω). This means that the measured resistance should be constant, independent of the probe spacing d. The experimental data points for the $\sqrt{3} \times \sqrt{3}$-Ag surface in Fig. 5 roughly follow this tendency rather than Eq. (1). As described in detail in the next section, the $\sqrt{3} \times \sqrt{3}$-Ag surface has a two-dimensional free-electron like surface-state band which is metallic and conductive, and furthermore, its surface space-charge layer is always a hole-accumulation layer. This is why the surface region has a much higher conductivity than in the bulk [12]. The contribution from the surface-state band dominates the high conductance as revealed in the next section. Therefore, the conduction is two-dimensional, rather than three-dimensional.

In this way, by changing the probe spacing from macroscopic distances to microscopic ones, one can switch the conductivity measurement from the bulk-sensitive mode to surface-sensitive one, so that one can clearly distinguish between 2D conduction and 3D conduction.

4. Surface-state conduction

The $\sqrt{3} \times \sqrt{3}$-Ag surface is thus shown to have a much lower resistance, or much higher surface conductance than the 7×7 surface. Then, is this due to the surface-space charge layer or surface states? To answer this question, we shall first estimate the conductance through the space-charge layers under the respective surfaces. Since the Fermi-level position in the bulk is known from the impurity doping level (or the bulk resistivity), we have only to know the Fermi-level position at surface (E_{Fs}). Then we can calculate the band bending beneath the surface and the resulting carrier concentration there, to obtain the conductance through the surface space-charge layer [13]. The solid curve in Fig. 6 shows the space-charge-layer conductance of our sample crystal. The conductance on vertical axis is shown with respect to that under flat-band condition (where E_{Fs} coincides with E_F in the bulk). When E_{Fs} is located around the middle of bulk band gap, the surface space-charge layer is a depletion layer where the conductance is low. When E_{Fs} is near the bulk conduction-band minimum (valence-band maximum E_V), the layer is an electron (hole) accumulation layer where the conductance is increased due to the excess carriers in the layer.

Fortunately, E_{Fs} positions at the 7×7 and $\sqrt{3} \times \sqrt{3}$-Ag surfaces are already known from photoemission spectroscopy measurements [10–12], 0.63 eV and 0.1–0.2 eV above E_V, respectively. These do not depend on the bulk doping level due to the Fermi-level pinning by metallic surface states. From Fig. 6, then, one can estimate the conductance through the surface space-charge layer below the respective surfaces. Since the 7×7 surface is located in the depletion region and the $\sqrt{3} \times \sqrt{3}$-Ag is in a weak hole-accumulation region, the latter surface should have a higher conductance than the former one. To compare this calculation result with the experimental data, the measured conductances for the respective surfaces are plotted in Fig. 6; dots with a bold line show the conductance of the $\sqrt{3} \times \sqrt{3}$-Ag surface with respect to that of the 7×7 surface, obtained from the data in Fig. 5. The data for the 7×7 surface is on the calculated curve: the detail of data processing is described in the caption of Fig. 6. The data points for the $\sqrt{3} \times \sqrt{3}$-Ag surface are located significantly above the calculated curve. Especially for the probe spacing less than 10 μm, the measured conductance is higher than the expected space-charge layer conductance by about one order of magnitude. As a conclusion, the measured high conductance of this surface cannot be explained only by the surface-space-charge-layer conductance, instead, the surface-state conductance contributes dominantly to the measured conductance.

The surface-state conductance of this surface was already detected with macroscopic four-point probe method by observing a conductance increase due to carrier doing into the surface-state band [14]. But the microscopic four-point probe method described above has made it possible just by comparing the conductance values between the two surfaces. This is owing to its high sensitivity in measurements of the surface-state electrical conduction [3]. In other words, the microscopic four-point probes whose probe spacing is comparable to the thickness of the space-charge layer is an effective tool for detecting and measuring the surface-state conductance of the topmost atomic layers. In spite of continuous efforts to detect the surface-state conductance since 1970s, unambiguous experimental detections have been

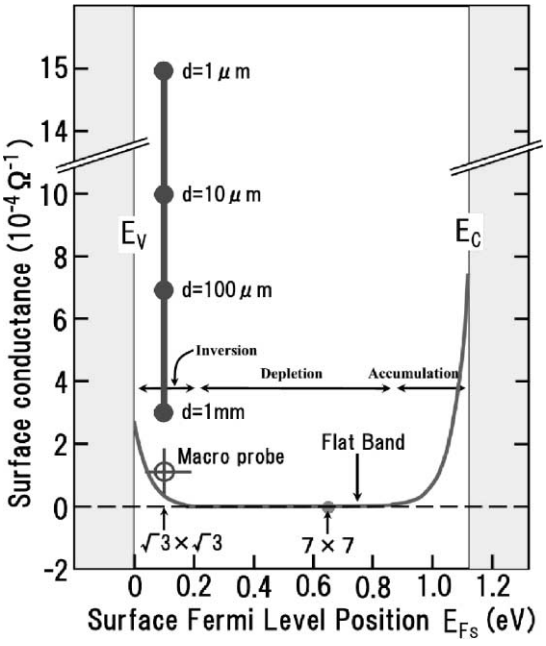

Fig. 6. The curve shows conductance through the surface space-charge layer, calculated as a function of surface Fermi level position (E_{Fs}). The calculation is done only for E_{Fs} within the band gap. The conductance on the vertical axis is shown with respect to that under the flat-band condition. To compare this calculated conductance with the experimental data, one has to know first the E_{Fs} position of each surface, which is fortunately already measured by photoemission spectroscopy. The E_{Fs}'s for the 7×7 and $\sqrt{3} \times \sqrt{3}$-Ag surfaces are 0.63 and 0.1–0.2 eV above the bulk valence-band maximum E_V, respectively [10,12]. Since the calculated conductance is not absolute values, but just a change from that under the flat-band condition, we cannot make straightforward comparison between the calculated conductance and the experimental data. Therefore, we next have to assume that the measured conductance of the 7×7 clean surface is the space-charge-layer conductance only; no surface-state conductance contributes. Then the data point of the 7×7 surface is right on the calculated curve at $E_{Fs} = 0.63$ eV above E_V. Since, then, we can obtain the difference in conductance between the 7×7 and $\sqrt{3} \times \sqrt{3}$-Ag surfaces from their measured conductance, we can plot the result at the E_{Fs} position of the $\sqrt{3} \times \sqrt{3}$-Ag surface, which is indicated by bold straight line with black circles. As shown in Fig. 5, the conductance changes in a wide range depending upon the probe spacing. As the probe spacing is reduced, the measured conductance significantly deviates upwards from the calculated curve. Therefore, the high conductance of the $\sqrt{3} \times \sqrt{3}$-Ag surface is not explained only by the space-charge-layer conductance, rather the surface-state conductance dominantly governs the measured value. If the assumption mentioned above about conductance of the 7×7 surface is not true, that is, if the surface-state conductance largely contribute to the measured conductance for the 7×7 surface, its data point should be located above the calculated curve. Then the data points for the $\sqrt{3} \times \sqrt{3}$-Ag surface also deviate further upwards above the calculated curve. This means again that the contribution from the surface-state conductance is further larger. Therefore, the above assumption does not affect the conclusion of the surface-state conductance of the $\sqrt{3} \times \sqrt{3}$-Ag surface, rather it makes an underestimation for its surface-state conductance. Though there are reports that the surface-state conductance of the 7×7 surface is 10^{-6}–10^{-8} Ω^{-1} [15,16], the conductance is lower than that of the $\sqrt{3} \times \sqrt{3}$-Ag surface by 2–4 orders of magnitudes, which is negligibly low. In any cases, the conclusion about the $\sqrt{3} \times \sqrt{3}$-Ag surface is not affected by whether the surface-state conductance contributes on the 7×7 surface.

lacking for a long time [6]. Therefore, the results described above are of significant importance in surface physics, which opens a new opportunity of study on transport property of surface electronic states.

For comparison, a data point obtained by a macroscopic four-point probe (probe spacing being about 10 mm) is plotted as an open circle in Fig. 6 [9]. Since this point is located close to the calculated curve, we can not say within the experimental errors that the data point deviate significantly from the calculated curve. Therefore, we could not conclude the contribution of the surface-state conductance just by comparing the measured conductance between the 7×7 and $\sqrt{3} \times \sqrt{3}$-Ag surfaces in the case of macro-four-point probe method [9]. This is because the macro-probe method does not enable precise measurements of surface-state conductance for lack of sufficient surface sensitivity.

5. Concluding remarks

Microscopic four-point probe methods described here are quite unique and power tools for surface science, especially for study of surface transport, and are expected to be increasingly important because the electrical conduction through one or two atomic layers on surfaces may play essential roles in nanometer-scale science and technology. The readers can feel their usefulness from the preliminary results described here. Of course, the probes can be applied not only for study of surface transport, but also for transport properties of microscopic and nanometer-scale objects. The probes will be used under various conditions such as at low and high temperatures, under magnetic field, and under light illuminations. We have already constructed a system for the micro-four-point probe measurements at temperatures down to 10 K in UHV. The results will be reported elsewhere.

Acknowledgements

The present work was done under Grand-in-Aid from the Ministry of Education, Science, Culture, and Sports of Japan, including International Collaboration Program. The four-tip STM prober was constructed during Core Research for Evolutional Science and Technology of the Japan Science and Technology Corporation.

References

[1] For review S. Hasegawa et al., Prog. Surf. Sci. 60 (1999) 89; J. Phys. C: Cond. Matter 12 (2000) R463.
[2] I. Shiraki et al., Surf. Rev. Lett. 7 (2000) 533.
[3] C.L. Petersen et al., Appl. Phys. Lett. 77 (2000) 3782.
[4] I. Shiraki et al., Surf. Sci. 493 (2001) 643.

[5] For review S. Hasegawa, I. Shiraki, F. Tanabe, F. Grey, Oyo Buturi 70 (2001) 1165 (The Japan Society of Applied Physics, in Japanese).
[6] M. Henzler, in: J.M. Blakely (Ed.), Surface Physics of Materials I, Academic Press, New York, 1975, p. 241.
[7] P. Boggild et al., Rev. Sci. Instrum. 71 (2000) 2781; Adv. Mater. 12 (2000) 947.
[8] For review S. Hasegawa et al., Jpn. J. Appl. Phys. 39 (2000) 3815.
[9] C.-S. Jiang, S. Hasegawa, S. Ino, Phys. Rev. B 54 (1996) 10389.
[10] F.J. Himpsel, G. Hollinger, R.A. Pollak, Phys. Rev. B 28 (1983) 7014.
[11] J. Viernow et al., Phys. Rev. B 57 (1998) 2321.
[12] S. Hasegawa et al., Surf. Sci. 386 (1997) 322.
[13] For fundamentals of semiconductor surfaces, e.g. W. Moench, Semiconductor Surfaces and Interfaces, Springer, Berlin, 1995.
[14] Y. Nakajima et al., Phys. Rev. B 56 (1997) 6782; Phys. Rev. B 54 (1996) 14134.
[15] Y. Hasegawa et al., Surf. Sci. 358 (1996) 32.
[16] S. Heike et al., Phys. Rev. Lett. 81 (1998) 890.